

4H-Silicon Carbide PN Diode for Harsh Environment Temperature Sensing Applications

Nuo Zhang



Electrical Engineering and Computer Sciences
University of California at Berkeley

Technical Report No. UCB/EECS-2014-103

<http://www.eecs.berkeley.edu/Pubs/TechRpts/2014/EECS-2014-103.html>

May 16, 2014

Copyright © 2014, by the author(s).
All rights reserved.

Permission to make digital or hard copies of all or part of this work for personal or classroom use is granted without fee provided that copies are not made or distributed for profit or commercial advantage and that copies bear this notice and the full citation on the first page. To copy otherwise, to republish, to post on servers or to redistribute to lists, requires prior specific permission.

4H-Silicon Carbide PN Diode for Harsh Environment Temperature Sensing Applications

by

Nuo Zhang

A report submitted in partial satisfaction of the

requirements for the degree of

Master of Science

in

Engineering – Electrical Engineering and Computer Sciences

in the

Graduate Division

of the

University of California, Berkeley

Committee in charge:

Professor Albert P. Pisano, Chair

Professor Tsu-Jae King Liu

Spring 2014

**4H-Silicon Carbide PN Diode for Harsh Environment Temperature Sensing
Applications**

by

Nuo Zhang

Research Project

Submitted to the Department of Electrical Engineering and Computer Sciences,
University of California at Berkeley, in partial satisfaction of the requirements for the
degree of **Master of Science, Plan II**.

Approval for the Report and Comprehensive Examination:

Committee:

Professor Albert P. Pisano
Research Advisor

(Date)

* * * * *

Professor Tsu-Jae King Liu
Second Reader

(Date)

4H-Silicon Carbide PN Diode for Harsh Environment Temperature Sensing Applications

Copyright © 2014

by

Nuo Zhang

Abstract

4H-Silicon Carbide PN Diode for Harsh Environment Temperature Sensing Applications

by

Nuo Zhang

Master of Science in Electrical Engineering and Computer Sciences

University of California, Berkeley

Professor Albert P. Pisano, Chair

Temperature sensing under harsh environments is important to various industrial applications, such as automotive industries, gas turbines, aerospace systems and deep-well drilling telemetric systems. Among different types of temperature sensors, semiconductor diode sensors have the advantages of high sensitivity and compatibility with integrated circuits.

Silicon carbide is a promising semiconductor material for harsh environment sensing applications thanks to its superior material properties compared with silicon and other semiconductor materials. The wide bandgap, high thermal conductivity, and high breakdown field allow SiC based devices to work under extreme conditions.

In this work, a temperature sensor based on 4H-SiC pn diode has been designed, fabricated and characterized. The device is capable of stable operation in a temperature range from 20 °C up to 600 °C. In the forward biased region, the forward voltage of the 4H-SiC pn diode shows linear dependence on temperature at a constant current. This dependence is utilized to sense temperature variations and the proposed device achieves a high sensitivity of 3.5 mV/°C. These results indicate that an integrated circuit compatible

temperature sensor based on 4H-SiC pn diode is a promising technology for harsh environment sensing applications.

Professor Albert P. Pisano
Research Advisor

TABLE OF CONTENTS

List of Figures	ii
List of Tables	iii
List of Abbreviations	iv
Chapter 1 Introduction	1
1.1 Harsh Environment Sensing Applications.....	1
1.2 Material Properties of Silicon Carbide	3
1.2.1 Crystal Structure.....	3
1.2.2 Material Properties	5
1.3 Temperature Sensing Technology	6
1.4 Temperature Sensors Based on SiC Diodes	8
1.5 Thesis Organization.....	8
Chapter 2 Fundamentals of PN Junction Diode and Sensing Mechanism	10
2.1 Fundamentals of PN Junction Diode	10
2.1.1 PN Junction Electrostatics Under Equilibrium.....	10
2.1.2 Current Conduction Mechanisms	12
2.2 Temperature Sensing Mechanism.....	14
Chapter 3 Sensor Design and Fabrication Process	16
3.1 Sensor Design	16
3.2 Fabrication Process	17
Chapter 4 Measurement Results and Performance Evaluation	19
4.1 Current-Voltage Measurement at Different Temperatures.....	19
4.2 Evaluation of the Temperature Sensor.....	21
Chapter 5 Conclusion and Future Work	24
5.1 Conclusion	24
5.2 Future Work.....	25
Bibliography	26

LIST OF FIGURES

Figure 1-1. Tetrahedrally bonded Si-C cluster [5], [6].	3
Figure 1-2. Hexagonal close packing positions of Si-C bilayers [5], [8].	4
Figure 1-3. Stacking sequences of Si-C bilayers along c-axis for 3C-, 4H-, and 6H-SiC [8].	5
Figure 1-4. High temperature applications and desired sensing measurands.	7
Figure 2-1. Conceptual pn junction and equilibrium energy band diagram.	12
Figure 3-1. Cross-sectional schematic of the temperature sensor based on 4H-SiC pn diode.	17
Figure 3-2. Fabrication process flow for the temperature sensor.	18
Figure 3-3. SEM image of the fabricated temperature sensor based on 4H-SiC pn diode.	18
Figure 4-2. I-V measurement of the 4H-SiC pn diode based temperature sensor at different temperatures (20 – 600 °C).	20
Figure 4-1. High temperature probe station made by Signatone.	20
Figure 4-3. Measured forward voltage versus temperature at different forward current densities.	21
Figure 4-4. Measured and modeled sensitivity versus forward current density of the 4H-SiC pn diode temperature sensor. The extracted ideality factor and carrier lifetime are indicated on the graph.	22

LIST OF TABLES

Table 1-1. High temperature electronic applications [2]. BS stands for bulk silicon technology, SOI stands for silicon on insulator technology, WBG stands for wide bandgap semiconductor technology and NA stands for currently not available.....	2
Table 1-2. Material properties of Si, GaAs and SiC [7]. \perp indicates perpendicular to c-axis, and \parallel indicates parallel to c-axis.	6

LIST OF ABBREVIATIONS

Al	Aluminum
C	Carbon
D_N	Diffusion coefficient of electrons
D_P	Diffusion coefficient of holes
E_g	Energy bandgap
ϵ_0	Vacuum permittivity
ϵ_s	Relative permittivity
GaAs	Gallium arsenide
k	Boltzmann constant
L_N	Diffusion length of electrons
L_P	Diffusion length of holes
N_A	Doping concentration of p-type semiconductor
N_D	Doping concentration of n-type semiconductor
N_C	Effective density of conduction band states
N_V	Effective density of valance band states
n	Ideality factor
n_i	Intrinsic carrier concentration
Ni	Nickel
PECVD	Plasma enhanced chemical vapor deposition
q	Electric charge
RIE	Reactive ion etch
RTD	Resistance temperature detector
RTA	Rapid thermal annealing

SEM	Scanning electron microscope
Si	Silicon
SiC	Silicon carbide
SiO ₂	Silicon dioxide
SOI	Silicon-on-insulator
T	Temperature
TCP	Transformer coupled plasma
Ti	Titanium
τ_e	Effective carrier lifetime
V _{bi}	Built-in potential
W _{dep}	Depletion width

Chapter 1

Introduction

1.1 Harsh Environment Sensing Applications

Harsh environment conditions are defined as one or more of the following: high temperatures, high shock or intense vibration, high radiation, erosive and corrosive conditions [1]. An integrated sensing module capable of operating under those extreme conditions would be beneficial to a number of industrial applications, such as automotive industries, aerospace systems, industrial turbines and deep-well drilling telemetric systems [2], [3]. The ability to place a sensing unit at the crucial hot spots enables real-time monitoring of the systems. Consider industrial turbines as an example. Combustion or steam turbines are the necessary devices to convert thermal energy into electricity. It is important to monitor a variety of physical parameters within the hot sections of the turbines in order to increase turbine efficiency, reliability and to reduce pollution [4]. In addition, real-time monitoring can help to detect and predict the failures of critical components in a timely fashion to reduce the maintenance costs of the systems.

Table 1-1. High temperature electronic applications [2]. BS stands for bulk silicon technology, SOI stands for silicon on insulator technology, WBG stands for wide bandgap semiconductor technology and NA stands for currently not available.

High Temperature Electronic Applications	Peak Ambient (°C)	Current Technology	Future Technology
Automotive			
Engine Control Electronics	150	BS & SOI	BS & SOI
On-cylinder & Exhaust Pipe	600	NA	WBG
Electric Suspension & Breaks	250	BS	WBG
Electric/Hybrid Vehicle PMAD	150	BS	WBG
Turbine Engine			
Sensors, Telemetry, Control	300	BS & SOI	SOI & WBG
	600	NA	WBG
Electric Actuation	150	BS & SOI	WBG
	600	BS	WBG
Spacecraft			
Power Management	150	BS & SOI	WBG
	300	NA	WBG
Venus & Mercury Exploration	550	NA	WBG
Industrial			
High Temperature Processing	300	SOI	SOI
	600	NA	WBG
Deep-Well Drilling Telemetry			
Oil and Gas	300	SOI	SOI & WBG
Geothermal	600	NA	WBG

Among all the harsh environment conditions, the devices that can stand high temperature have drawn lots of attention due to numerous applications listed in Table 1-1 [2]. Silicon (Si) based devices cannot survive at high temperatures ($> 300\text{ }^{\circ}\text{C}$) mainly due to the high intrinsic carrier concentration which exceeds the intentional doping, and high leakage currents. Silicon-on-insulator (SOI) technology enables silicon devices to approach their theoretical limits by cutting off leakage paths. At temperatures higher than $300\text{ }^{\circ}\text{C}$, wide bandgap semiconductors provide solutions capable of exceeding the limits of Si. Therefore, they are indicated as future technologies in Table 1-1.

1.2 Material Properties of Silicon Carbide

SiC-based semiconductor electronic devices and circuits are being developed for working under extreme conditions, such as high temperature, high power, and high radiation. This is thanks to its superior material properties compared with Si and other semiconductors. This section briefly surveys the basic properties and advantages of SiC material.

1.2.1 Crystal Structure

SiC is a group IV-IV compound semiconductor. Each silicon (Si) atom is tetrahedrally bonded with four carbon (C) atoms, and vice versa. The approximate distance between Si-C atoms is 1.89 \AA , and the distance between Si-Si or C-C atoms is 3.08 \AA . The tetrahedrally bonded Si-C cluster is shown in Figure 1-1 [5], [6].

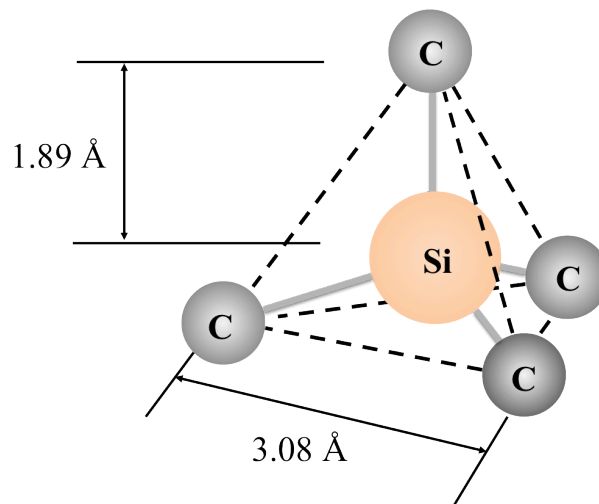


Figure 1-1. Tetrahedrally bonded Si-C cluster [5], [6].

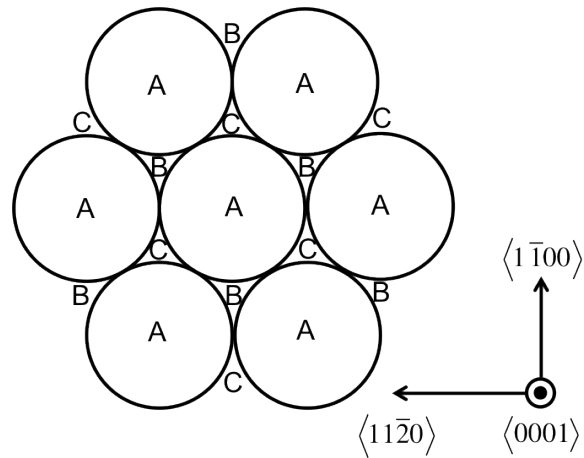


Figure 1-2. Hexagonal close packing positions of Si-C bilayers [5], [8].

SiC exists in many different crystal structures with the same chemical composition, called polytypes [5]-[8]. There are over 100 known polytypes of SiC, and the most common polytypes of SiC that have been developed for electronic applications are 3C-SiC, 4H-SiC, and 6H-SiC.

Considering the Si-C pair as a sphere, they form hexagonal patterns when packed closely in a plane as a Si-C bilayer. The positions of the spheres in the first plane are denoted as A-site positions. For the next layer packed on top of the first layer, it can take either B-site positions or C-site positions. The hexagonal packing positions of Si-C bilayers are shown in Figure 1-2. Different polytypes are composed of different stacking sequences of Si-C bilayers. For instance, 4H-SiC has a stacking sequence of ABCB and it repeats every four layers throughout the crystal. Similarly, 6H-SiC has a stacking sequence of ABCACB. Both 4H-SiC and 6H-SiC have hexagonal crystal structures. 3C-SiC, sometimes referred to as β -SiC, has a stacking sequence of ABC and it is the only form of SiC with a cubic crystal structure. The schematic structures of common polytypes of SiC are shown in Figure 1-3.

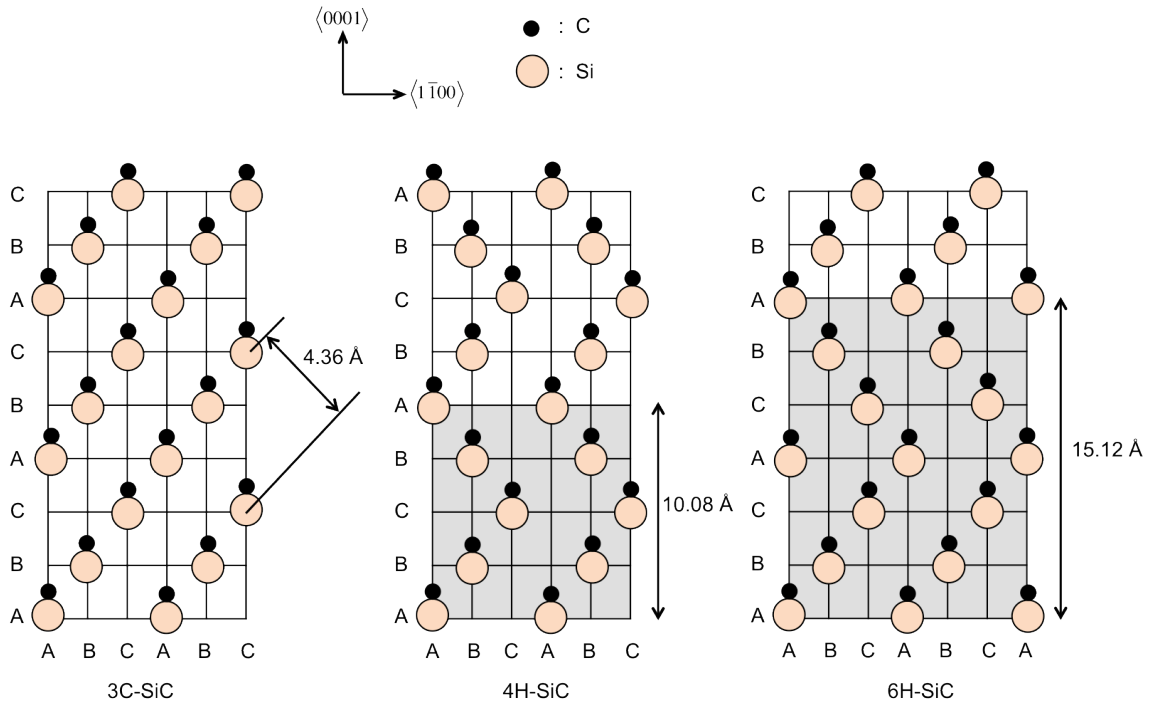


Figure 1-3. Stacking sequences of Si-C bilayers along c-axis for 3C-, 4H-, and 6H-SiC [8].

1.2.2 Material Properties

SiC is a promising semiconductor for harsh environment sensing applications due to its excellent electrical and physical properties [1]-[10]. The wide bandgap energy and low intrinsic carrier concentration allow SiC based semiconductor devices to be functional at much higher temperatures. Moreover, high breakdown field, high-saturated electron velocity, and high thermal conductivity enable SiC devices to work under extreme conditions. The basic material properties of three SiC polytypes are summarized in Table 1-2 [7]. The critical field and mobility of SiC are anisotropic, and they strongly depend on crystallographic directions of applied electric field and current flow. For comparison, the properties of Si and gallium arsenide (GaAs) are also included in Table 1-2. 4H-SiC is used in this work thanks to the widest energy bandgap.

Table 1-2. Material properties of Si, GaAs and SiC [7]. \perp indicates perpendicular to c-axis, and \parallel indicates parallel to c-axis.

Property	Si	GaAs	3C-SiC	6H-SiC	4H-SiC
Energy Bandgap [eV]	1.12	1.42	2.3	3.0	3.2
Critical Field at $N_D = 10^{17} \text{ cm}^{-3}$ [MV/cm]	0.6	0.6	1.8	\parallel 3.2 \perp >1	\parallel 3.0 \perp 2.5
Thermal Conductivity [W/cmK]	1.5	0.5	3-5	3-5	3-5
Saturated Electron Drift Velocity [10^7 cm/s]	1.0	1.2	2.5	2.0	2.0
Electron Mobility at $N_D = 10^{16} \text{ cm}^{-3}$ [cm^2/Vs]	1200	6500	750	\parallel 60 \perp 400	\parallel 800 \perp 800
Hole Mobility at $N_A = 10^{16} \text{ cm}^{-3}$ [cm^2/Vs]	420	320	40	90	115
Relative Dielectric Constant	11.9	13.1	9.7	9.7	9.7

1.3 Temperature Sensing Technology

Temperature sensor is an important component of the integrated sensing module and it is desired in many high temperature applications. Figure 1-1 shows the high temperature applications and desired sensing measurands. There is a wide variety of existing temperature sensors with different sensing mechanisms. Common temperature sensors include thermocouples, thermistors, resistance temperature detectors (RTDs), infrared sensors, optical sensors and semiconductor diodes [9].

Thermocouples are the most widely used temperature sensors in industry. A thermocouple is formed by joining two dissimilar metal alloy wires. It indicates temperature by measuring a change in voltage, and a reference junction is needed during this process. Thermocouples usually have wide operational range (-250 – 1250 °C) but low accuracy.

Thermistors, often made from ceramics or polymers, take advantage of the fact that

Energy Industries	Geothermal	Oil & Gas Exploration	Industrial Gas Turbines	Aircraft Engines	Automotive Engines
Required Sensing Temperatures	 374°C	 275°C	 600°C	 600°C	 300°C
Desired Sensing Measurands	<ul style="list-style-type: none"> • Pressure • Temperature • H₂S • Strain 	<ul style="list-style-type: none"> • Pressure • Temperature • Hydrocarbon • Strain 	<ul style="list-style-type: none"> • Pressure • Temperature • Flame speed • Acceleration 	<ul style="list-style-type: none"> • Pressure • Temperature • Flame speed • Acceleration 	<ul style="list-style-type: none"> • Pressure • Temperature • Flame speed • O₂

Figure 1-4. High temperature applications and desired sensing measurands.

the resistance of materials changes with temperature. They usually exhibit a large resistance change over a small temperature range (-90 – 130 °C) and therefore have high accuracy.

RTDs also measure the change of resistance in order to indicate temperature variation. However, they consist of metal wires coiled around small diameter ceramic cylinders. They have high accuracy and wide temperature range (-200 – 500 °C). However, they are known to be fragile especially in harsh environments.

Infrared sensors indicate temperature from a portion of the thermal radiation emitted by the object being measured. They are non-contact sensors, which means no physical touch is needed when measuring the temperature. However, it is tricky to apply the infrared sensor to obtain accurate temperature measurement.

There are many other types of temperature sensors, such as optical sensors, capacitive sensors and semiconductor diodes. Each type of the temperature sensors has potential benefits for specific applications. One key design of the temperature sensors in

the harsh environment sensing modules is the ease of integrating the sensors with the supporting circuitries. For a harsh environment temperature sensor that can be easily integrated with other circuit components, a temperature sensor based on SiC diode is desired and investigated in this work.

1.4 Temperature Sensors Based on SiC Diodes

SiC Schottky diodes have been previously demonstrated as viable temperature sensors that can work up to 400 °C [11]-[13]. However, SiC Schottky diode suffers from reliability issues of the Schottky contact as well as high leakage current at elevated temperatures. On the other hand, SiC pn junction is very stable and theoretically permits device operation at junction temperatures exceeding 800 °C [7]. Hence, the temperature sensor based on SiC pn diode is a perfect candidate for operation at elevated temperatures [14].

1.5 Thesis Organization

This work focuses on development and characterization of a high-performance temperature sensor based on 4H-SiC pn diode that is capable of operating in a temperature range from 20 °C up to 600 °C. This report consists of five chapters including this introduction. In chapter 2, a discussion of the fundamentals of pn junction diode and the sensing mechanism are discussed. Chapter 3 presents the design of the device structure and details the fabrication process. Chapter 4 discusses the experimental

results. Finally, the contributions of this work are summarized and suggestions for future research directions are proposed in chapter 5.

Chapter 2

Fundamentals of PN Junction Diode and Sensing Mechanism

2.1 Fundamentals of PN Junction Diode

A pn junction is formed between two regions in a single crystal of semiconductor material with different doping concentrations. PN junctions are of great importance in modern electronics. They are the basic building blocks of most semiconductor devices. It is essential to know the fundamentals of pn junction diode in order to understand the sensing mechanism of the temperature sensor. In this section, the electrostatics under equilibrium is first discussed. The subsequent segments are then devoted to current conduction mechanisms and current-voltage characteristics.

2.1.1 PN Junction Electrostatics Under Equilibrium

Suppose that the p- and n- regions are initially separated. Then a structurally perfect connection is made between these two regions. Since there are more holes in the p-region

than in the n-region, the holes tend to diffuse into the n-side. As holes diffuse, they leave behind ionized acceptors, which are immobile (fixed within semiconductor lattice sites). Likewise, electrons from the n-region near the metallurgical junction begin to diffuse into the p-region, leaving fixed ionized donors in the n-region. Consequently, the near-vicinity of the metallurgical junction loses their neutrality and holds a significant non-zero charge, forming the space charge region or depletion region. The diffusion process generates space charge, whereas the drift current associated with the electric field generated by the space charge counteracts the diffusion. The build-up of charge continues until the carrier diffusion and drift components balance each other out. Then the equilibrium condition is established. A conceptual pn junction and the energy band diagram under equilibrium are illustrated in Figure 2-1. The voltage drop across the depletion region under equilibrium conditions is called *built-in potential* (V_{bi}) [16].

$$V_{bi} = \frac{kT}{q} \ln \left(\frac{N_A N_D}{n_i^2} \right), \quad (2.1)$$

where q is the electric charge, k is Boltzmann constant, T is the temperature in Kelvin, N_D and N_A are the doping concentrations in n- and p-region, $n_i = \sqrt{N_C N_V} e^{-\frac{E_g}{2kT}}$ is the intrinsic carrier concentration.

The total width of the space-charge or depletion region, also known simply as the *depletion width*, is given by

$$W_{dep} = \left[\frac{2\epsilon_s \epsilon_0}{q} \left(\frac{N_A + N_D}{N_A N_D} \right) V_{bi} \right]^{1/2}, \quad (2.2)$$

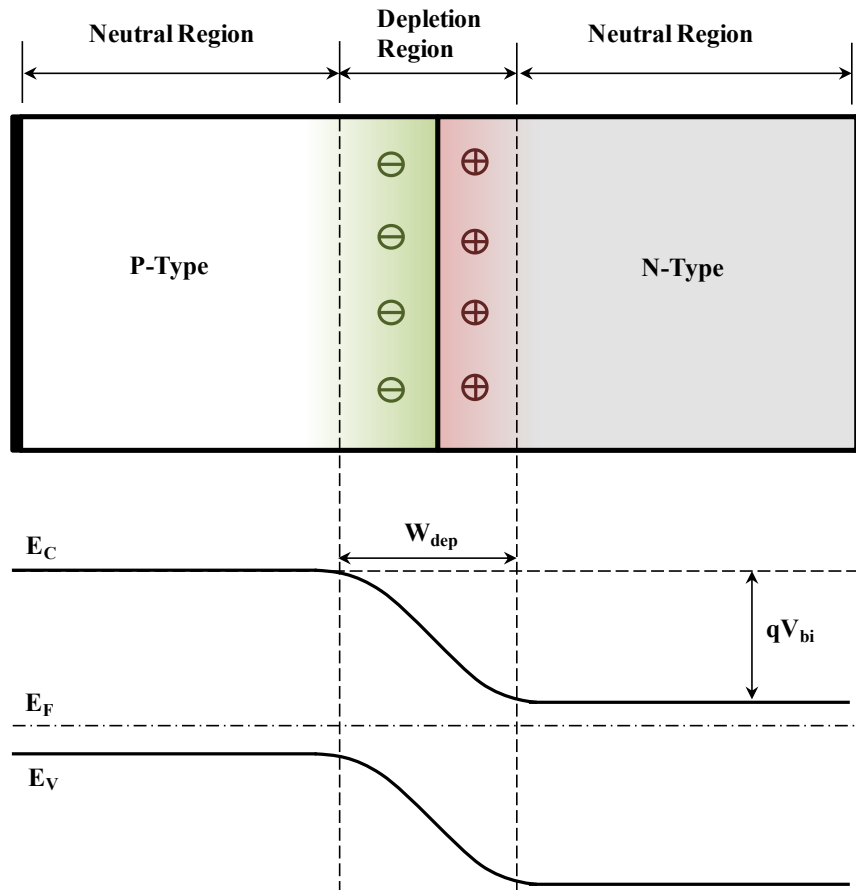


Figure 2-1. Conceptual pn junction and equilibrium energy band diagram.

where ϵ_s is the relative permittivity of the semiconductor material, and the ϵ_0 is the vacuum permittivity.

2.1.2 Current Conduction Mechanisms

Several current transport mechanisms may occur at the same time in pn diodes. The ideal current-voltage characteristics are derived by Shockley [17] based on four assumptions: (1) the pn junction is abrupt; (2) Boltzmann approximation is valid throughout the depletion layer; (3) the injected minority carrier densities are much smaller than the majority carrier densities; (4) no generation in the depletion region. The

current describe by the ideal diode equation is commonly referred to as the *diffusion current*.

However, the measurement results usually differ from the prediction by the ideal diode equation. One of the important effects that are responsible for the departure from the ideal is the generation and recombination of carriers in the depletion region. Wolf *et al.* [18] first reported that the current-voltage characteristics of Si pn diode could be more accurately resented by a double exponential relationship of the form

$$J_{total} = J_{0,diff} \left[\exp\left(\frac{qV_D}{n_1 kT}\right) - 1 \right] + J_{0,rec} \left[\exp\left(\frac{qV_D}{n_2 kT}\right) - 1 \right], \quad (2.3)$$

where J_{total} is the total current density, $J_{0,diff}$ is the saturation current density for diffusion, $J_{0,rec}$ is the saturation current density for recombination in the depletion region, n_1 and n_2 are ideality factors. $n_1 = 1$ for the case of ideal diffusion current. The value of n_2 depends on the location of the recombination centers within the bandgap. Typically, the expected n_2 is close to 2.

In addition to the generation and recombination in the depletion region, there are other non-ideal effects: (1) the surface effect; (2) the tunneling current via multiple defect sites; (3) the high-level injection effect (the injected minority carrier density is comparable to the majority carrier concentration); (4) the series resistance. The relative strength of the different current mechanisms depends on the properties of semiconductor materials, dopants, and the defects.

2.2 Temperature Sensing Mechanism

The diffusion current and the recombination current are the most important two current mechanisms in the temperature sensor based on 4H-SiC pn diode. At forward bias ($qV_F \gg kT$), a general form of the current density J_F of the pn diode at a given applied bias-voltage V_F can be then expressed using the following equation [14]-[16]:

$$J_F = J_0 e^{\frac{qV_F}{nkT}}, \quad (2.4)$$

where q is the electric charge, k is Boltzmann constant, n is the ideality factor and has a value between 1 and 2.

When the diffusion current dominates, $n = 1$ and

$$J_0 = qN_C N_V \left(\frac{D_N}{L_N N_A} + \frac{D_P}{L_P N_D} \right) e^{-\frac{E_g}{kT}}, \quad (2.5)$$

where N_C and N_V are the effective density of conduction and valence band states, D_N and D_P are the diffusion coefficients of electrons and holes, L_N and L_P are the diffusion lengths of electrons and holes, N_D and N_A are the doping concentrations in N-SiC and P-SiC, E_g is the bandgap energy. For 4H-SiC, the bandgap is 3.23 eV at 300 K. The effective density of states in the conduction band N_C and valence band N_V can be calculated from

$$N_C = 3.25 \times 10^{15} \times T^{3/2} \text{ cm}^{-3}, \quad (2.6)$$

$$N_V = 4.85 \times 10^{15} \times T^{3/2} \text{ cm}^{-3}. \quad (2.7)$$

When the recombination current dominates, $n = 2$ and

$$J_0 = \frac{qn_i W_{dep}}{2\tau_e}, \quad (2.8)$$

where n_i is the intrinsic carrier concentration, W_{dep} is the depletion width, and τ_e is the effective carrier lifetime.

Typically, recombination current dominates at low current levels in 4H-SiC pn diode, showing $n = 2$ [14], [15]. At forward bias ($qV_F \gg kT$), the forward voltage of the pn diode can be calculated by

$$V_F = \frac{2kT}{q} \ln\left(\frac{J}{J_0}\right) = \frac{2kT}{q} \ln\left(\frac{2J\tau_e}{qW_{dep}}\right) - \frac{kT}{q} \ln(N_C N_V) + \frac{E_g}{q}. \quad (2.9)$$

If the temperature dependence of τ_e , W_{dep} , N_C and N_V is negligible, the theoretical sensitivity of the temperature sensor based on 4H-SiC pn diode can be expressed as [14], [15]

$$\frac{dV_F}{dT} \approx \frac{2k}{q} \ln\left(\frac{2J\tau_e}{qW_{dep}}\right) - 7.67mV / K. \quad (2.10)$$

Chapter 3

Sensor Design and Fabrication Process

3.1 Sensor Design

The temperature sensor is based on 4H-SiC pn diode structure. The cross-sectional view of the device is illustrated in Figure 3-1. The n-region is formed by a 1- μm -thick N+ 4H-SiC epitaxial layer doped at 10^{19} cm^{-3} , and the p-region is formed by a 0.3- μm -thick P 4H-SiC layer doped at $1.8 \times 10^{18} \text{ cm}^{-3}$. Both pn diode terminals are accessible at the top for easy circuit integration. The device is electrically isolated by a lightly doped N-region epitaxially grown on 4H-SiC substrate. The dimension of the metal contact pads is $130 \mu\text{m} \times 130 \mu\text{m}$, and the dimension of the N+ SiC mesa is $150 \mu\text{m} \times 150 \mu\text{m}$. The active area of the device is $2.25 \times 10^{-4} \text{ cm}^2$.

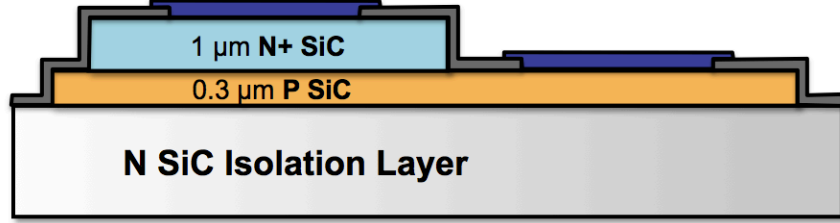


Figure 3-1. Cross-sectional schematic of the temperature sensor based on 4H-SiC pn diode.

3.2 Fabrication Process

The temperature sensors were fabricated using surface micro-machining techniques. The devices were fabricated on 4° off-axis Si-face n-type 4H-SiC wafer purchased from SiCrystal AG. And the epitaxial layers were grown by Ascatron AB. The detailed fabrication process flow is shown in Figure 3-2. First, a transformer coupled plasma (TCP) etching of N+ SiC epitaxial layer was performed using deposited silicon dioxide (SiO₂) layer as hard mask to define the N-type-mesa. Next, a second TCP etching of P-type SiC epitaxial layer was used to isolate the device. Then, plasma enhanced chemical vapor deposition (PECVD) of SiO₂ was performed for surface passivation. After that, the passivation oxide was patterned using reactive ion etch (RIE). E-beam evaporation was then used to deposit Ni for N-type SiC contacts, and Ni/Ti/Al metal stack for P-type SiC contacts. After each metal deposition, a lift-off process was used to pattern the contacts, and a rapid thermal annealing (RTA) step at high temperature was performed to obtain low resistive ohmic contacts. The specific contact resistances for N+ SiC and P SiC are $1.38 \times 10^{-4} \Omega\text{cm}^2$ and $2.18 \times 10^{-3} \Omega\text{cm}^2$, respectively. Figure 3-3 shows the scanning electron microscope (SEM) image of the fabricated temperature sensor.

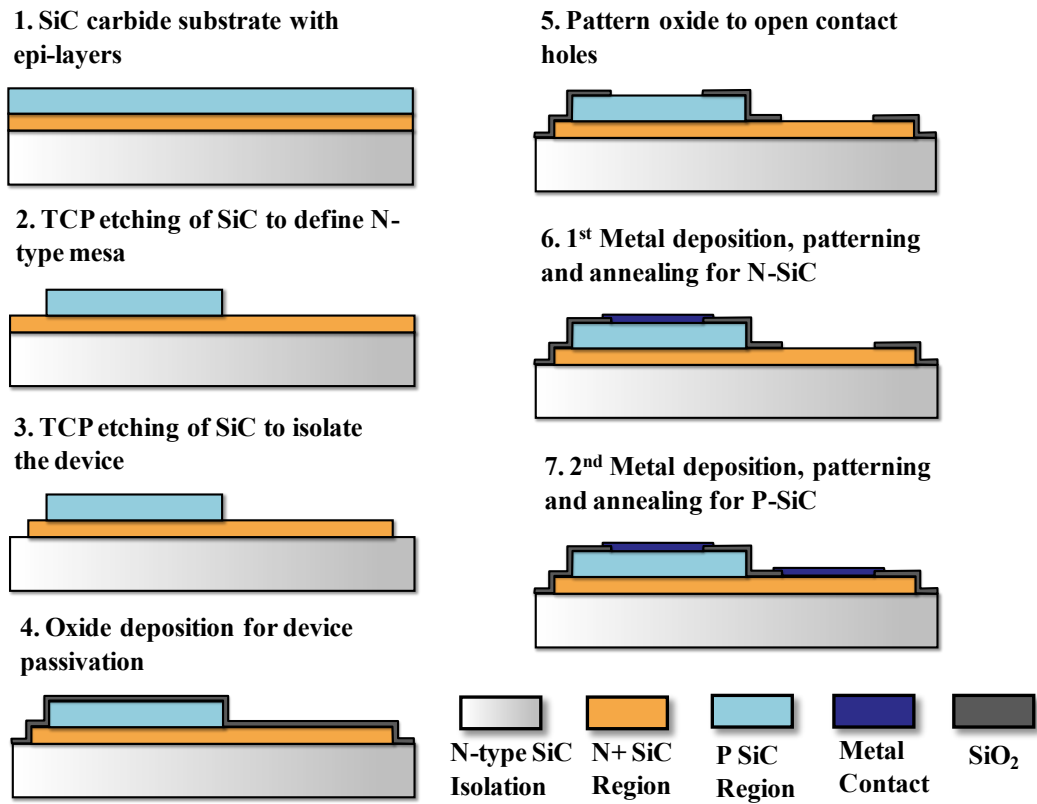


Figure 3-2. Fabrication process flow for the temperature sensor.

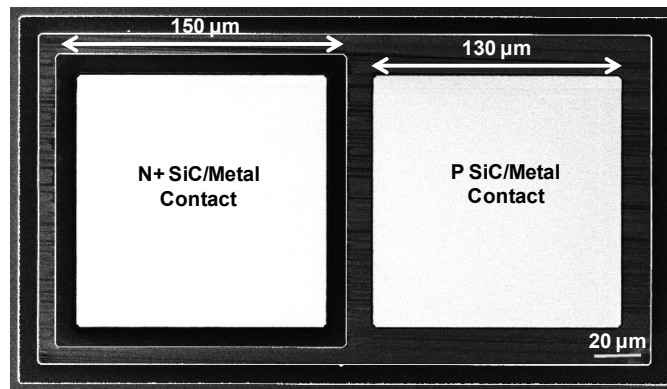


Figure 3-3. SEM image of the fabricated temperature sensor based on 4H-SiC pn diode.

Chapter 4

Measurement Results and Performance Evaluation

4.1 Current-Voltage Measurement at Different Temperatures

The current-voltage (I-V) characteristics of the fabricated device at different temperatures were measured by using a high temperature probe station made by Signatone together with an Agilent B2912A Precision Source/Measurement Unit. The high temperature probe station is shown in Figure 4-1. It consists of a ceramic hot chuck, a temperature controller and a water cooler. The probe station is capable of heating up to 600 °C. Figure 4-2 presents the I-V measurement results of the device from room temperature up to 600 °C. The peak temperature was not limited by the device, but by the high-temperature probe station. The figure shows that, by taking advantages of SiC material properties, stable device performance can be achieved at extremely high temperatures. From Figure 4-2, the ideality factor n of the fabricated device at low current levels was extracted to be 2.08 under room temperature and has a low variation of

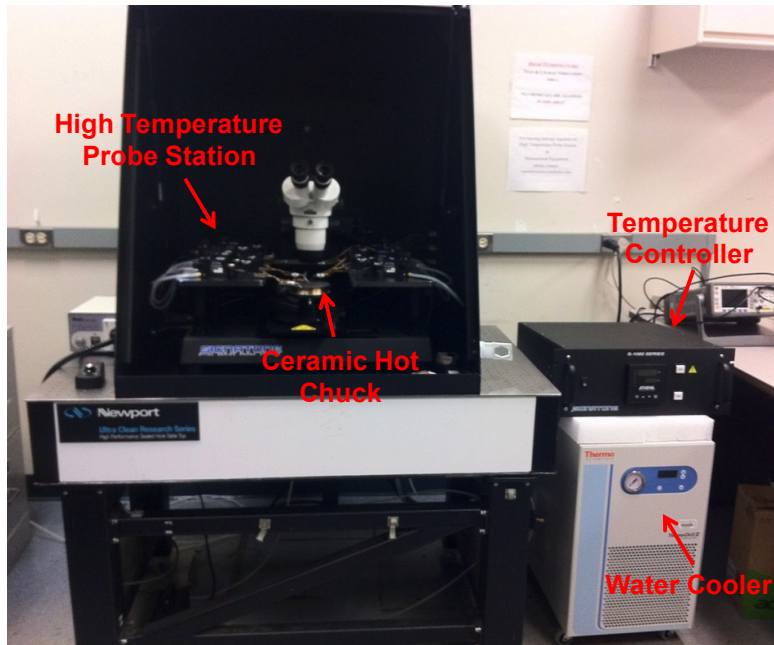


Figure 4-1. High temperature probe station made by Signatone.

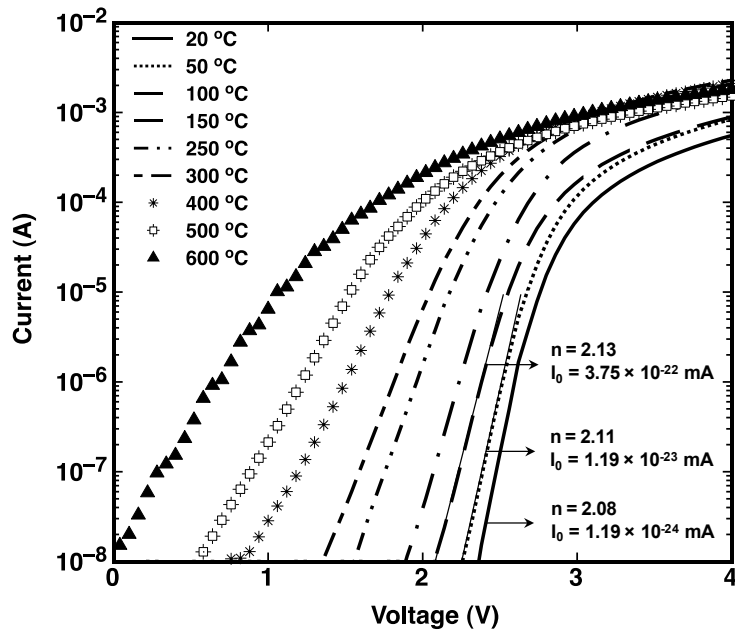


Figure 4-2. I-V measurement of the 4H-SiC pn diode based temperature sensor at different temperatures (20 – 600 °C).

around 15% over the temperature range. The extracted ideality factors and leakage currents at 20 °C, 50 °C and 100 °C are indicated on the graph. For a given forward current level, the voltage decreases with increasing temperature.

4.2 Evaluation of the Temperature Sensor

Figure 4-3 illustrates the forward voltage versus temperature of the fabricated device at different forward current densities, respectively. The graph shows that the forward voltage of the device has a linear temperature dependence at all forward current levels, and it decreases with increasing temperature. By calculating the slopes of these linear relationships, temperature sensitivities can be obtained. At a forward current density of 0.44 A/cm², a sensitivity of 2.3 mV/°C is achieved. At a lower current density

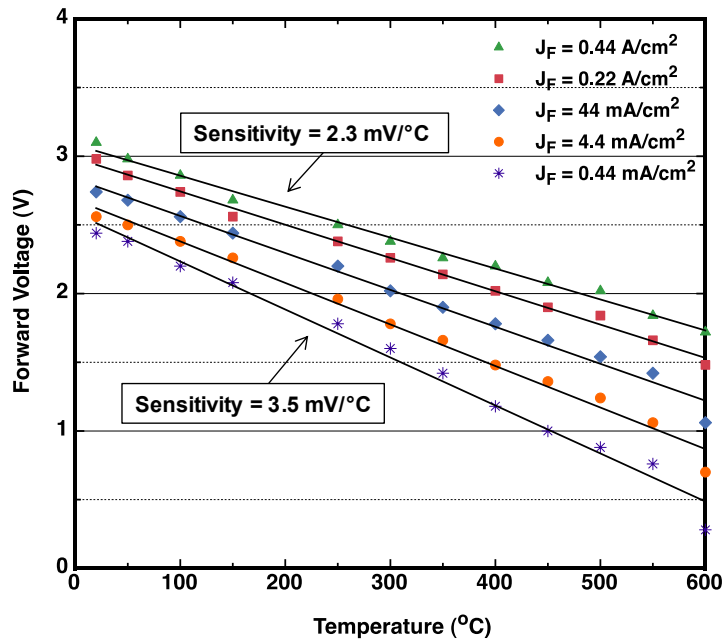


Figure 4-3. Measured forward voltage versus temperature at different forward current densities.

of 0.44 mA/cm^2 , the sensitivity increases to $3.5 \text{ mV/}^\circ\text{C}$. From Equation (2.10), it can be observed that the absolute value of dV_F/dT , which is the sensitivity, is higher at lower current level.

Figure 4-4 shows the sensitivity versus forward current density relationship. A linear relationship is observed, and $n = 2.0$ can be extracted from the slope of the fitted curve showing that recombination current dominates the current flowing in the 4H-SiC pn diode in the measured current range. The results show a good agreement with the model described in Equation (2.10). Given the doping concentrations of the N+ and P regions, the corresponding depletion width is $0.047 \text{ }\mu\text{m}$. The carrier lifetime $\tau_e = 0.167 \text{ ns}$ can also be extracted from the sensitivity versus forward current density relationship. The low carrier lifetime is mainly caused by the high density of interface traps between the

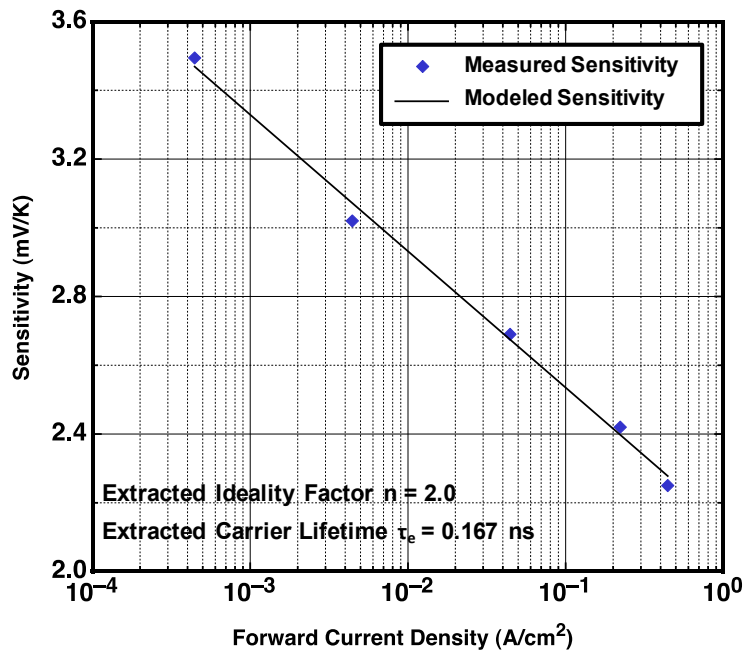


Figure 4-4. Measured and modeled sensitivity versus forward current density of the 4H-SiC pn diode temperature sensor. The extracted ideality factor and carrier lifetime are indicated on the graph.

passivation oxide and SiC.

In addition, the experimental results indicate that the proposed 4H-SiC pn diode achieves better sensitivities and higher operation temperatures in comparison with previously reported devices based on SiC Schottky diodes structures [11]-[13]. The sensitivity of the proposed device is also higher than the reported 4H-SiC pn diode betavoltaic cell [15] mainly due to the smaller depletion width and less impact of shunt resistance. The forward bias sensing mode can be used in the entire range from 20 °C to 600 °C and the forward voltage can be converted into a measurable variable by using a sensing circuit [11].

Chapter 5

Conclusion and Future Work

5.1 Conclusion

This work has demonstrated theoretical analysis and experimental results for a high-performance temperature sensor based on 4H-SiC pn diode. Fabrication process of the device was discussed in details. Thanks to the superior material properties of SiC, the temperature shows stable operation from room temperature up to 600 °C. Under forward bias condition, the temperature sensitivity of the sensor changes from 2.3 mV/K at a forward current density of 0.44 A/cm², to 3.5 mV/K at a forward current density of 0.44 mA/cm². Higher sensitivity can be achieved at a lower forward current level. The experimental results indicate a good agreement with the theoretical analysis. The device shows the potential to be integrated with supporting circuitries to build a sensing module for harsh environment applications.

5.2 Future Work

There are several technical challenges worth investigating to optimize the device performance. A further analysis on the influences of the design parameters, such as doping concentrations and thicknesses of the epitaxial layers, can be developed for achieving higher sensitivity. For the fabrication process, the metallization step is vital for high temperature operation of the temperature sensor based on 4H-SiC pn diode. In this work, Ni is used for N-type SiC contacts and Ni/Ti/Al metal stack is used for P-type SiC contacts. Though both contacts showed stable operation up to 600 °C, long-term stability test should be performed to study the electrical behaviors of the contacts. To further extend the operating temperature of the device, more metals need to be explored, especially for P-type SiC contacts. TiW is a strong candidate that is very stable at high temperatures and could work for both N-type and P-type SiC.

Bibliography

1. M.B.J. Wijesundara and R.G. Azevedo, *Silicon Carbide Microsystems for Harsh Environments*, New York: Springer, 2011.
2. P. G. Neudeck, R. S. Okojie, and L. -Y. Chen, "High-temperature electronics - a role for wide bandgap semiconductors," *Proceedings of IEEE*, vol. 90, pp. 1065-1076, Jun. 2002.
3. D. G. Senesky, B. Jamshidi, K. B. Cheng, and A. P. Pisano, "Harsh environment silicon carbide sensors for health and performance monitoring of aerospace systems: a review," *IEEE Sensors Journal*, vol. 9, pp. 1472-1478, Nov. 2009.
4. X. Gong, L. An, and C. Xu, "Wireless passive sensor development for harsh environment applications," *2012 IEEE International Workshop on Antenna Technology (iWAT)*, pp. 140-143, Mar. 2012.
5. C. -M. Zetterling, *Process technology for silicon carbide devices*, London: IEE, 2002.
6. H. -S. Lee, *Fabrication and Characterization of Silicon Carbide Power Bipolar Junction Transistors*, Doctorial Thesis, Department of Microelectronics and Applied Physics (MAP), KTH, Royal Institute of Technology, Stockholm, Sweden, 2008.
7. K. H. J. Bushchow, R. W. Cahn, M. C. Flemings, B. Ilshner, E. J. Kramer, S. Mahajan, and P. Veyssiere Eds., *Encyclopedia of Materials: Science and Technology*, New York: Elsevier, 2001.
8. H. Miyake, *Interface Control of AlGaIn/SiC Heterojunction and Development of High-Current-Gain SiC-Based Bipolar Transistors*, Ph.D. dissertation, Electronic Science and Engineering, Kyoto University, Japan, 2012.
9. S. Wodin-Schwartz, *MEMS Materials and Temperature Sensors for Down Hole Geothermal System Monitoring*, Ph.D. dissertation, Department of Mechanical Engineering, University of California, Berkeley, California, USA, 2013.
10. N. Zhang, Y. Rao, N. Xu, A. Maralani, and A. P. Pisano, "Characterization of 4H-SiC bipolar junction transistor at high temperatures," *Material Science Forum*, vol. 778-780, pp. 1013-1016, 2014.
11. F. Draghici, M. Badila, G. Brezeanu, I. Rusu, F. Craciunoiu, I. Enache, "An industrial temperature probe based on SiC diodes," *2010 International Semiconductor Conference (CAS)*, vol. 2, pp. 409-412, 2010.

12. I. Josan, C. Boianceanu, G. Brezeanu, V. Obreja, M. Avram, D. Puscasu, A. Ioncea, "Extreme environment temperature sensor based on silicon carbide Schottky diode," *2009 International Semiconductor Conference (CAS)*, vol. 2, pp. 525-528, 2009.
13. R. Pascu, F. Draghici, M. Badila, F. Craciunoiu, G. Brezeanu, A. Dinescu, I. Rusu, "High temperature sensor based on SiC Schottky diodes with undoped oxide ramp termination," *2011 International Semiconductor Conference (CAS)*, vol. 2, pp. 379-382, 2011.
14. N. Zhang, C. -M. Lin, D. G. Senesky, and A. P. Pisano, "Temperature sensor based on 4H-silicon carbide pn diode operational from 25°C to 600°C," *Applied Physics Letters*, vol. 104, 073504, Feb. 2014.
15. M. V. S. Chandrashekhar, R. Duggirala, M. G. Spencer, and A. Lal, "4H SiC betavoltaic powered temperature transducer," *Applied Physics Letters*, vol. 91, 053511, Aug. 2007.
16. S. M. Sze, *Physics of Semiconductor Devices*, 2nd Edition, New York: Wiley, 1981.
17. W. Shockley, "The theory of $p-n$ junctions in semiconductors and $p-n$ junction transistors," *Bell System Technical Journal*, vol. 28, pp. 435-489, Jul. 1949.
18. M. Wolf, G. T. Noel, and R. J. Stirn, "Investigation of the double exponential in the current-voltage characteristics of silicon solar cells," *IEEE Transactions on Electron Devices*, vol. 24, pp. 419-428, Apr. 1977.